35th AIAA Fluid Dynamics Conference and Exhibit
Toronto, ON, June 6-9 2005 AIAA-2005-5269

# Feedback Control of Cavity Flow Using Experimental Based Reduced Order Model

E. Caraballo[1], X. Yuan[2], J. Little[1], M. Debiasi[1], P. Yan[2], A. Serrani[2], J. H. Myatt[3], and M. Samimy[1,§]

*Collaborative Center for Control Science*
*The Ohio State University, Columbus, Ohio*

[1]Dept. of Mechanical Eng., The Ohio State University

[2]Dept. of Electrical and Computer Eng., The Ohio State University

[3] Air Force Research Laboratory Air Vehicles Directorate

[§]Corresponding author, E-mail: samimy.1@osu.edu

**We present preliminary results on subsonic cavity flow control using reduced-order model based feedback control derived from experimental measurements. The reduced-order model was developed using the Proper Orthogonal Decomposition of PIV results in conjunction with the Galerkin projection of the Navier-Stokes equations onto the resulting spatial eigenfunctions. The stochastic estimation method was used for real-time estimate of the model time coefficients from dynamic surface pressure measurements. Equilibrium analysis led to the linearization of the reduced-order model around the equilibrium point and a model for controller design was obtained by shifting the origin of the coordinates to the equilibrium point. A linear-quadratic optimal controller was then designed and tested in the experiments. The results obtained are very promising and show that control is capable of reducing the cavity flow resonance not only at the Mach 0.3 flow, for which the reduced-order model was specifically derived, but also at other flows with some variation of the Mach number. These preliminary results indicate that the control switches the flow from a single mode resonance to a multi-mode resonance.**

## I. Introduction

Closed-loop control has proven to be very successful for enhancing the performance of complex systems and in the recent past various attempts have been made to use it in flow control (Gad-El-Hak 2000, Cattafesta et al. 2003). In contrast with open-loop flow control, which can produce useful results but lacks the flexibility and robustness needed for application in dynamic flight environments, closed-loop flow control appears to be a good candidate technique for the successful flow management in many applications. However, the tools of classical control systems theory are not directly applicable to the fluid flow systems which are governed by the Navier-Stokes equations and display non-linear behavior and pose formidable modeling challenges due to their infinite dimensionality and their complexity. Therefore, in order to design and successfully implement a closed-loop control strategy, it is necessary to obtain simpler models of the flow systems, which capture their important dynamic characteristics as well as the effect of the actuation.

This is one of the goals of the flow control group at the Collaborative Center of Control Science at The Ohio State University and this paper presents the progress made in developing and experimentally testing a reduced-order model based controller for suppression of intense cavity flow pressure fluctuations. This phenomenon is characterized by a strong coupling between the flow and acoustic that produces intense resonant pressure fluctuations. This strong resonant flow, which could adversely affect store separation and also cause structural damage to adjacent surfaces, is well documented and represents an interesting and challenging benchmark for testing closed-loop flow control strategies. A comprehensive review of this flow and of different control and actuation strategies developed for its suppression are given by Cattafesta et al. (2003). Past works by the same authors document the characteristics of cavity flow specific to the experimental apparatus used in this study and present some interesting open-loop and closed-loop control techniques that have proven to be very effective in reducing cavity flow noise (Debiasi and Samimy 2004, Samimy et al. 2004, and Yuan et al. 2005).

The current work continues and expands the studies previously done by the same authors using numerical data (Caraballo et al 2003, Caraballo et al 2004). Similar to the previous studies, a reduced-order model was obtained using the snapshot based Proper Orthogonal Decomposition (POD) technique in conjunction with the Galerkin projection of the Navier-Stokes equations onto the POD modes. The main difference is that the current reduced-order model and the attendant control are based on experimental (PIV) rather than numerical data. In addition, the reduced-order based controller was successfully implemented in the experiment.

The state of the reduced-order model (i.e. the POD time coefficients) was estimated in real-time by employing the stochastic estimation technique with correlations obtained from simultaneous particle image velocimetry (PIV) and dynamic pressure measurements at several locations on the surface of the cavity. This is similar to the approach introduced by Glauser et al. (2004) for controlling the separation of the flow over an airfoil.

Equilibrium analysis led to the linearization of the reduced-order model around the equilibrium point. A simpler model for controller design was then obtained by shifting the origin of the coordinates to the equilibrium point. This corresponds to removing the effect of the mean flow from the low-order model, and considering the local behavior of the system around the mean flow. The availability of real-time estimates of the state of the model allowed the use of linear state feedback control. To this aim we designed and tested experimentally a linear-quadratic optimal state feedback controller. From the results obtained we can conclude that the controller significantly reduces the resonance peak of the Mach 0.3 single Rossiter mode, for which it was designed, by switching it to a multi-mode resonance. The controller seems to be quite robust, as it can control the flow with some variations in the flow Mach number. It should be emphasized that these results, while quite exciting, are preliminary. Further analysis, interpretation, and development are forthcoming.

In the next sections we will introduce the flow facility used in this study and then focus on the POD and Galerkin methods adopted for deriving the reduced-order model and the stochastic estimation approach used for real-time estimate of the model variables directly from dynamic pressure measurements. This is followed by the design and application of the linear-quadratic controller and presentation and discussion of the results.

## II. The experimental facility

We used the experimental facility described in detail in Debiasi and Samimy (2004). This is an instrumented, optically accessible wind-tunnel operating in a blow-down fashion with atmospheric exhaust. The filtered, dried air is conditioned in a stagnation chamber before entering a smoothly contoured converging nozzle to the 2 inch by 2 inch test section. The facility can run continuously in the subsonic range between Mach 0.25 and 0.70 and transonic and supersonic applications are possible by changing modular components.

A shallow cavity with a depth $D$ = 12.7 mm and length $L$ = 50.8 mm for a length to depth aspect ratio $L/D$ = 4 is recessed in the floor of the test section. For control the cavity shear-layer receptivity region is forced by a 2-D synthetic-jet type actuator issuing at 30 degrees relative to the main flow from a 1 mm slot embedded in the cavity leading edge and spanning the width of the cavity, Fig 1. A Selenium D3300Ti compression driver provides the mechanical oscillations necessary to create the zero net mass, non-zero net momentum flow for actuation. The actuator signals are produced by either a BK Precision 3011A function generator for open-loop forcing or by a dSPACE 1103 DSP control board in closed-loop studies and are amplified by a Crown D-150A amplifier.

Particle Image Velocimetry (PIV) has been used to capture “snapshots” of the flow field under different uncontrolled (baseline) and controlled conditions, Fig. 2. Images are acquired and processed using a LaVision Inc. PIV system. The main flow is particle seeded with Di-Ethyl-Hexyl-Sebacat (DEHS) particles by using a 4-jet atomizer upstream of the stagnation chamber. This location allows homogenous dispersion of the submicron particles throughout the test section. A dual-head Spectra Physics PIV-400 Nd:YAG laser operating at the 2nd

harmonic (532 nm) is used in conjunction with spherical and cylindrical lenses to form a thin (~1mm), vertical sheet spanning the streamwise direction of the cavity at the middle of test section width. In order to minimize beam reflections, a small slot cut into the cavity floor allows the laser sheet to exhaust and diffuse in a sealed light-trap. The time separation between the lasers pulses used to illuminate the DEHS particles can be tuned according to the flow velocity. For Mach 0.30 flow this value is 1.8 microseconds. Two images corresponding to the pulses from each laser head were acquired by a 2000 by 2000 pixel CCD camera equipped with a 90mm macro lens with a narrow band-pass optical filter. The images were divided into 32 by 32 pixel interrogation windows which contained 6-10 DEHS particles each. For each image sub regions were cross correlated by using multi-pass processing with 50% overlap. The resulting vector fields were post-processed to remove any remaining spurious vectors. This setup gave a velocity vector grid of 128 by 128 over the measurement domain of 50.8 mm which translates to each velocity vector being separated by approximately 0.4 mm.

Flush-mounted Kulite transducers placed on various locations on the cavity and on the walls of the test section were used for dynamic pressure measurements. Figure 3 shows the locations of the transducers used in this study. These transducers have an almost flat frequency response up to about 50 kHz and are powered by a dedicated signal conditioner that amplifies and low-pass filters at 10 kHz their signals. When dynamic pressure traces are acquired simultaneously with PIV global velocity measurements, each transducer is protected by a thin Teflon shield that prevents contamination from the flow seed. The effect of this shield is a reduction of the transducers sensitivity at higher frequencies. We verified that, in the frequency range 1-10 kHz relevant in this study for flow control, the sensitivity reduction caused by the shield is inconsequential.

For state estimation, dynamic pressure measurements were recorded simultaneously with PIV measurements by using a National Instruments (NI) PCI-6143 S-Series data acquisition board mounted on a Dell Precision Workstation 650 that allows synchronous sampling of 8 channels with a maximum sampling frequency of 250 kHz per channel. Each pressure recording is band-pass filtered between 800 Hz and 10 kHz to remove spurious frequency components. In the current study 500 PIV snapshots were recorded for each flow/actuation condition explored. For each PIV snapshot 256 pressure samples from the laser Q-switch signal and from each of the transducers of Fig. 3 were acquired at 50 kHz. The NI board was triggered by a programmable timing unit (PTU) housed in the PIV system that activated the beginning of the acquisition to allow the Q-switch TTL to fall approximately in the middle of the 256 data points. The simultaneous sampling of the laser Q-switch signal with the pressure signals allows for each snapshot the identification of the section of pressure timetraces corresponding to the instantaneous PIV velocity field. Additional, longer recordings of 262,144 samples per channel acquired at 200 kHz were also used to derive SPL spectra as described in Debiasi et al. (2004).

For closed-loop control of the flow a dSPACE 1103 DSP board connected to the Dell Precision Workstation 650 was used. This system utilizes four independent, 16-bit A/D converters each with 4 multiplexed input channels and allows simultaneous acquisition and control processing of 4 signals and almost simultaneous, due to multiplexing, acquisition and processing of additional signals at a rate up to 50 kHz per channel to produce at the same rate a control signal from a 14-bit output channel. Similar to state estimation pressure data, the pressure signals were band-pass filtered between 800 Hz and 10 kHz to remove spurious frequency components.

## III. Reduced-order Modeling

The reduced-order model derived for controller design is based on PIV and surface pressure measurements of the cavity flow. A total of 500 snapshots of the two component velocity field were taken simultaneously with surface pressure measurements at 4 locations in the cavity wall. The procedure for deriving a low dimensional model for control has been presented by the authors in previous works (Samimy et al. 2004, and Caraballo et al. 2004). The approach is based on the POD method to obtain a spatial basis of the flow. The POD method is combined with the Galerkin projection method to obtain the temporal coefficients required in the POD expansion. Stochastic estimation is used to estimate the temporal coefficients based on real time surface pressure measurements.

### POD Method

More details on the fundamentals of this method, introduced by Lumley (1967) as an objective way to extract large scale structures in a turbulent flow, can be found in Berkooz et al. (1993), Holmes et al. (1996) and Delville et al. (1998). In its original formulation the method requires a very large number $\mathcal{T}$ of time resolved data set at a number $\mathcal{L}$ of spatial locations ($\mathcal{T} >> \mathcal{L}$); as the number of spatial locations is increased, the problem becomes more complex. The POD method aims to describe the temporal-spatial evolution of the fluctuating components of the

flow variables (e.g. the fluctuating component $u$' of the streamwise velocity $u$) as combination of $N < \mathcal{L}$ spatial modes (or eigenfunctions) $\varphi_i(\boldsymbol{x})$, i.e. a reduced basis of modes that capture the coherent structures, the dominant features, present in the flow:

$$u'(\boldsymbol{x},t) \cong \sum_{i=1}^{N} a_i(t)\varphi_i(\boldsymbol{x}) \quad . \tag{3.1}$$

The time coefficients $a_i(t)$ are functions of time only and capture the time evolution of the corresponding coherent structures. The number $N$ of modes used depends on the nature of the problem. The temporal behavior of the modes can be recovered by obtaining the time coefficients for each of the modes from:

$$a_i(t) = \int_D u'(\boldsymbol{x},t)\varphi_i^*(\boldsymbol{x})\,d\boldsymbol{x} \tag{3.2}$$

where * denotes complex conjugate. Obviously, to calculate the time coefficients, the instantaneous flow field has to be measured or numerically calculated simultaneously at every point in the flow domain of interest.

The POD approach used in this investigation is the snapshot method of Sirovich (1987) which is an alternative way of obtaining the POD modes more suitable for highly spatially resolved data sets ($\mathcal{L} >> \mathcal{T}$) that can be obtained using numerical simulations or advanced laser based flow diagnostics. This approach provides a representation of the flow similar to Eqn. (3.1) with $N << \mathcal{T}$. A detailed description of the application of the Sirovich POD method to the current study case is given in Samimy et al. (2004) and Caraballo et al. (2004).

For this preliminary work, 500 PIV snapshots of the flow field were acquired as described in the previous section and used for deriving the modes and their time coefficients. Using 500 snapshots the average turbulent kinetic energy of the flow for the baseline Mach 0.3 case didn't completely converge in the shear layer region. However, the shape of the individual modes as well as the energy distribution of each mode didn't change using 300 or more snapshots, especially for the lower order dominant modes.

**Galerkin Projection and Low Dimensional Model**

The Galerkin projection method was used to obtain a reduced-order model of the cavity flow consisting of a system of ordinary differential equations for the time coefficients $a(t)=[a_1(t)\ a_2(t)\ \ldots\ a_N(t)]$. The method relies on the projection of the governing equations of the flow, the compressible Navier-Stokes in this case, onto the basis of POD modes. Detailed explanation on the derivation of this model is given in Samimy et al. (2004) and Caraballo et al. (2004). The form of the equations used here is based on the work of Rowley (2002), where the compressible Navier-Stokes equations are simplified and written as:

$$\begin{aligned} &\frac{Dc}{Dt} + \frac{\gamma - 1}{2} c\,\nabla \bullet \boldsymbol{u} = 0 \\ &\frac{D\boldsymbol{u}}{Dt} + \frac{2}{\gamma - 1} c\nabla c = \frac{\mu}{\rho}\nabla^2 \boldsymbol{u} \end{aligned} \tag{3.3}$$

where $\boldsymbol{u} = (u,v)$ is the velocity vector and $c$ is the local speed of sound.

To apply the Galerkin method, first each flow variable is decomposed into its mean and fluctuating components, and then the POD expansion equation (3.1) is written for each of the fluctuating components. Next, the flow variables in (3.3) are replaced by the expanded expressions of mean and fluctuating components. The new form of the governing equations is then projected onto the basis of POD modes by taking the inner product of each term with the POD modes according to the vector norm (Rowley, 2002). The resulting system of equations has the form:

$$\dot{a}(t) = F + Ga(t) + \begin{bmatrix} a^T(t)H^1 a(t) \\ \vdots \\ a^T(t)H^N a(t) \end{bmatrix}, \tag{3.4}$$

where $F$, $G$ and $H^i$, $i = 1,\ldots N$, are constant coefficients matrices obtained from the Galerkin projection. The number $N$ of modes used in the POD description of the flow defines the number of equations.

In the derivation of (3.4) the control input is not separated from the rest of the flow, i.e. the control effect is implicit in the model, which is not useful for control law design. In order to derive a model where the control input appears explicitly in the equations, the sub-domain of space where the control is introduced is separated from the rest of the field, as detailed in Efe et al. (2003a and 2003b), which yields a system in the following form:

$$\dot{a}(t) = F + Ga(t) + \begin{bmatrix} a^T(t)H^1 a(t) \\ \vdots \\ a^T(t)H^N a(t) \end{bmatrix} + B\Gamma(t) + \begin{bmatrix} \left(\overline{B}^1\Gamma(t)\right)^T a(t) \\ \vdots \\ \left(\overline{B}^N\Gamma(t)\right)^T a(t) \end{bmatrix}, \qquad (3.5)$$

where, similar to (3.4), the matrices of constant coefficients $F$, $G$, $H^i$, $B$ and $\overline{B}^i$, $i=1,\ldots N$, are obtained from the Galerkin projection, and $\Gamma$ is the control input applied at the forcing location, Yuan et al. (2005).

Equations (3.4) and (3.5) provide a model of the cavity flow in terms of the time coefficients $a(t)$ obtained with the POD method from $\mathcal{T}$ time uncorrelated PIV data sets. The modeling soundness of (3.5) was checked by solving it to obtain some time evolution of the coefficients for the baseline Mach 0.3 flow. The constant coefficients matrices of (3.5) and the initial values of $a(t)$ used to solve it were obtained as described above from PIV snapshots of this flow. The system was solved for different numbers of POD modes. When using 4 to 9 modes, the results converged and produced periodic time coefficients evolving in a bounded fashion independent of the initial conditions. The amplitude of oscillation of the coefficients is comparable to the values of the coefficients corresponding to the PIV snapshots (it is slightly higher using 4 modes, and slightly smaller for the other cases). Using less than three modes the solution didn't converge. Based on these results, we decided to adopt four modes for the model used to design the controller so to simplify the control algorithm and its experimental implementation.

## IV. Stochastic Estimation

The Stochastic Estimation (SE) was proposed by Adrian (1979) as another method to extract coherent structures from a turbulent flow field. The method estimates flow variables at any location by using the information, including statistical information, about the flow at a limited number $\mathcal{L}^*$ of locations. Several researchers have used SE to study various flows (e.g. Adrian and Moin 1988, Cole et al. 1991, Cole and Glauser 1998). Some have used it as a complementary technique to obtain POD time coefficients from experimental measurements, such as velocities or pressure, e.g. in subsonic jets (Picard and Delville, 2000) and in cavity flows (Murray and Ukeiley, 2003, and Samimy et al 2004). When used with POD, the stochastic estimation helps to recreate the state of the flow (a snapshot) for each time instant a measurement is taken. The estimated snapshot can then be used to calculate the corresponding estimated time coefficient with (3.2). The estimated time coefficient can be used as the initial condition to solve the Galerkin system (3.4) or (3.5) or to control the flow as will be explained in a later section.

In our study we obtain an estimate $\hat{a}(t)$ of the time coefficients $a(t)$ of (3.5) directly from the dynamic pressure measurements. With our experimental setup we obtain real-time measurements of the surface pressure at four locations of interest in the cavity test section (labeled 2, 3, 5, and 6 in Fig. 3). A quadratic stochastic estimation of the velocity field and of the time coefficient based on the surface pressure was obtained using the experimental data. The required pressure correlation matrices were obtained by averaging the value of the pressure correlation for the 500 timetraces of 256 pressure samples, obtained as described in section II. For the pressure-velocity correlations matrices and for the pressure-time coefficient correlation matrices, only the 500 pressure values simultaneous with the times of PIV capture were used. Then the time coefficients of the PIV images were obtained with (3.2). The procedure to obtain the estimation matrices is described in more detail in Caraballo et al. (2004).

For control purposes, as the controller is designed based on the Galerkin system (3.5), it is desirable to use SE to establish a relation between the time coefficients and these surface pressure measurements. The estimation can be written in the following form:

$$\hat{\boldsymbol{a}}_{\boldsymbol{i}}(\boldsymbol{t}) = \boldsymbol{C}_{\boldsymbol{ik}}\,\boldsymbol{p}_{\boldsymbol{k}}(\boldsymbol{t}) + \boldsymbol{D}_{\boldsymbol{ikl}}\,\boldsymbol{p}_{\boldsymbol{k}}(\boldsymbol{t})\,\boldsymbol{p}_{\boldsymbol{l}}(\boldsymbol{t}) \qquad i=1\ldots N, \qquad k, l\ldots=1\ldots\mathcal{L}^* \quad , \qquad (4.1)$$

where $C$, $D\ldots$ are the matrices of the estimation coefficients obtained by minimizing the average mean square error $e_i$ between the values of $a_i(t_r)$ at the times of PIV capture and the estimated ones $\hat{a}_i(t_r)$ at the same times,

$$e_i = \left\langle [\hat{a}_i(t_r) - a_i(t_r)]^2 \right\rangle \qquad r = 1 \ldots \mathcal{T}, \tag{4.2}$$

In evaluating the method with data from numerical simulation, Caraballo et al (2004) observed that retaining both the linear and the quadratic terms in Eqn. 4.1 significantly improved the results. Caraballo et al. used pressure values from four locations, three in the cavity floor and one in the cavity side wall, without optimizing their position or number. The results were good and thus a similar procedure is implemented experimentally in this study. Figure 4 compares the first four estimated time coefficients (thick red lines) to the values obtained with the POD method at the times of PIV capture (blue dots). For all four modes the amplitude of the estimated coefficients is close to the expected value.

## V. Controller Design and Implementation

Using the Galerkin model (3.5) obtained in Section III, and retaining the first 4 modes, we derived the following state space model for the baseline Mach 0.3 flow

$$\dot{a}(t) = F + Ga(t) + \begin{bmatrix} a^T(t)H^1 a(t) \\ \vdots \\ a^T(t)H^4 a(t) \end{bmatrix} + B\Gamma(t) + \begin{bmatrix} \left(\overline{B}^1\Gamma(t)\right)^T a(t) \\ \vdots \\ \left(\overline{B}^4\Gamma(t)\right)^T a(t) \end{bmatrix}, \tag{5.1}$$

to be used for control design. The reader is referred to Yuan et. al. (2005) for a detailed description of the coefficient matrices.

**Equilibrium analysis and model simplification**

As a first step in the design of a feedback control law for (5.1), we start with determining the equilibrium points of the unforced system, which corresponds to the solutions of the system of algebraic equations

$$f(a) = \underline{0}\ , \qquad f(a) = F + Ga(t) + \begin{bmatrix} a^T(t)H^1 a(t) \\ \vdots \\ a^T(t)H^N a(t) \end{bmatrix}. \tag{5.2}$$

Since this task involves solving a system of nonlinear algebraic equations, a numerical method must be employed. In our case, a Newton iterative algorithm is implemented to calculate the roots of (5.2) (Yuan et. al., 2005). The feasible solution of (5.2) that is, the solution that is compatible with the expected range of variation for the state *a* of the Galerkin system with *N*=4, is computed as

$$a_0 = [0.0227 \quad 0.3701 \quad 0.2901 \quad 0.5879]^T. \tag{5.3}$$

Then, the dynamics (5.1) has been linearized about the equilibrium point, to obtain the Jacobian linearization of the Galerkin system in the form

$$\dot{a} = J(a_0)\, a \quad , \qquad J(a_0) \equiv \left.\frac{\partial f(a)}{\partial a}\right|_{a=a_0}, \tag{5.4}$$

where $J(a_0)$ is the Jacobian matrix evaluated at the equilibrium. The eigenvalues of the Jacobian matrix have been computed as

$$\lambda\left(J\left(a_0\right)\right)=\begin{bmatrix} 0.1841+1.3386\mathrm{i} \\ 0.1841-1.3386\mathrm{i} \\ -0.0812 \\ -0.2840 \end{bmatrix}, \tag{5.5}$$

which shows the presence of two unstable eigenvalues for the linearized system. This implies, as expected, that the mean flow (corresponding to the equilibrium $a_0$) is an unstable solution for the Galerkin system.

To obtain a simpler model for controller design, the origin of the coordinate systems has been shifted to the equilibrium point $a_0$. Transforming the equilibrium of the system to the origin corresponds to removing the effect of the mean flow from the low order model, and considering the local behavior of the system around the mean flow. Letting

$$\tilde{a} = a - a_0 , \tag{5.6}$$

the model in the new set of coordinates $\tilde{a}$ reads as

$$\dot{\tilde{a}} = \tilde{G}\tilde{a} + \begin{bmatrix} \tilde{a}^T H^1 \tilde{a} \\ \vdots \\ \tilde{a}^T H^4 \tilde{a} \end{bmatrix} + B\Gamma + \begin{bmatrix} \left(\overline{B}^1\Gamma\right)^T \tilde{a} \\ \vdots \\ \left(\overline{B}^4\Gamma\right)^T \tilde{a} \end{bmatrix}, \tag{5.7}$$

where

$$\tilde{G} = G + \begin{bmatrix} a_0^T\left(H^1 + \left(H^1\right)^T\right) \\ \vdots \\ a_0^T\left(H^4 + \left(H^4\right)^T\right) \end{bmatrix}. \tag{5.8}$$

The modified model has the same structure as (5.1) but with the equilibrium shifted to the origin, which is more convenient for controller design and stability analysis.

**Linear quadratic state feedback control**

In the new coordinates, the Jacobian linearization of (5.7) at the origin is readily obtained as

$$\dot{\tilde{a}} = \tilde{G}\tilde{a} + B\Gamma . \tag{5.9}$$

Recall that the stochastic estimation method provides a way to estimate the time coefficients of the Galerkin system from real time pressure measurements, Eqn. (4.1). Therefore, the state of (5.9) can be estimated as

$$\hat{\tilde{a}}(t) = \hat{a}(t) - a_0 . \tag{5.10}$$

The availability of real-time estimates of the state of the Galerkin model (5.7) allows the use of linear state feedback control.

A convenient and well-established methodology for the controller design is offered by linear-quadratic (LQ) optimal control (Bertsekas, 1995). The control problem is cast as the minimization of the infinite-horizon cost function $J_c(\tilde{a},\Gamma)$ given by

$$J_c = \int_0^\infty \left(\tilde{a}^T W_{\tilde{a}} \tilde{a} + \Gamma^T W_\Gamma \Gamma\right) dt , \tag{5.11}$$

where $W_{\tilde{a}} > 0$ and $W_\Gamma > 0$ are a positive definite state weighting matrix and a positive scalar control weight, respectively. Minimization of $J_c$ results in having the trajectory $\tilde{a}(t)$ of the closed-loop system converging to zero minimizing a weighted functional of the control energy and the state. The tradeoff between minimization of the control energy and speed of convergence of $\tilde{a}(t)$ is determined by the choice of the weighting matrices $W_{\tilde{a}}$ and $W_\Gamma$, which play the role of control design parameters. In our final design, the weights have been chosen as $W_{\tilde{a}} = I_{4\times4}$ and $W_\Gamma = 10^4$, resulting in a much larger penalty on the control than on the state, required to obtain a small control effort. It is well known that the optimal control that minimizes the functional (5.11) is given by a linear function of the state trajectory $\tilde{a}(t)$, that is, a control law of the form

$$\Gamma = -K\hat{\tilde{a}}, \tag{5.12}$$

where *K* is a constant matrix, which in our case reads as

$$K = \begin{bmatrix} -16.7354 & -340.9832 & -85.3481 & 283.4039 \end{bmatrix}.$$

Applying the state feedback control (5.12) to the linearized system (5.9) results in mirroring all the unstable right half plane eigenvalues of the Jacobian matrix to the left half plane, as indicated in Fig. 5. Figure 6 shows the result of simulations obtained applying the state feedback control (5.12) to the finite-dimensional nonlinear model (5.1). It can be concluded that, at least in principle, the linear control (5.12) succeeds in stabilizing the equilibrium at origin of the four-mode Galerkin system (5.1).

Before presenting the experimental results, it is worth summarizing the structure of the model-based controller thus derived. As depicted in Fig. 7, the model-based controller design in this paper includes a stochastic estimation subsystem and a feedback from the estimated state. The former provides an estimate of the state $\hat{a}$ from real-time pressure measurements collected in different locations in the cavity, and the latter is the linear state feedback designed on the basis of the Jacobian linearization of the 4-dimensional Galerkin system. The linear state feedback matrix *K* acts on $\hat{\tilde{a}}$, which is the estimate of the state $\tilde{a}(t)$ obtained computing the deviation of the output of the stochastic estimator $\hat{a}(t)$ from the equilibrium $a_0$. The remaining blocks in figure 7 are a saturation function that limits the amplitude of the actuator, and a constant scaling factor $\alpha$, whose role will be clarified in the next section.

**Real time control results**

In this section, we summarize the results obtained in the real time experimental implementation of the state feedback controller depicted in Figure 7. It is important to point out that, to prevent damaging the actuator, the control input signal is limited to the range ± 7V. Since the gains of the LQ control (5.12) are quite large, a constant saturation of the actuator was observed during closed-loop experiments. Therefore, it was necessary to introduce a constant scaling factor $\alpha > 0$ in the feedback loop to keep the actuator below the saturation limits. The scaling factor, and the corresponding scaled control have been chosen as

$$\Gamma_\alpha(t) = -\alpha K\hat{\tilde{a}}(t) \qquad\qquad \alpha = 0.05. \tag{5.13}$$

The performance of the scaled control law (5.13) has been tested in closed-loop experiments for different flows in the neighborhood of Mach 0.3, our reference case for suppression of cavity flow resonance. Figure 8 shows an example of SPL reduction obtained by the controller. The thin (red) line is the SPL spectrum of the original unforced (baseline) flow, whereas the thick (black) line corresponds to the spectrum under LQ control. At Mach 0.27 and 0.3 the unforced flows exhibit a strong, single-mode resonant peak at about 2800 Hz whereas at Mach 0.32 the flow exhibits a multi-mode behavior. LQ control reduces by more than 15 dB the resonant peak at the design Mach number 0.30, Fig. 8 a). This is accompanied by a broadband SPL increase in the neighborhood of the second Rossiter mode at about 1900 Hz. There are some similarities between these results and those obtained using other linear output feedback controls, see e.g. Fig. 4 in Debiasi et al. 2004. The major difference is that we have induced a broadband fluctuation around the 2nd Rossiter mode here while a strong single Rossiter mode was observed with the output feedback controls (Debiasi et al. 2004). The same general characteristics and benefits are maintained when the control is applied to the lower Mach number flows with single-mode resonance like in the case of Mach 0.27

flow, Fig. 8 b). At Mach 0.32, a condition where the unforced flow has fully reached a multi-mode resonance state, Fig. 8 c), control is not beneficial and, while reducing the peak at 3300Hz, it increases the spectral peaks close to 2000 Hz.

It is clear from the closed loop system responses that the LQ state feedback can successfully reduce the dominant Rossiter peak and have good robustness under different flow conditions. Meanwhile, it is interesting to analyze the impact of the additional scaling factor $\alpha$ from the control systems point of view. As a matter of fact, the control objective of the LQ controller is to stabilize the linearized Galerkin model (5.9), which results in a much higher gain $K$ beyond the output range of the actuator. As depicted in Fig. 9, the LQ control with the scaling factor $\alpha$ is no longer a stabilizing controller because of the existence of two right-half plane closed-loop eigenvalues. On the other hand, the control $\Gamma_\alpha(t)$ does reduce the amplitude of the oscillations, which can be validated by applying the $\Gamma_\alpha(t)$ to the nonlinear Galerkin model (5.7) in simulations, Fig. 10. From the perspective of nonlinear analysis on the Galerkin model (5.7), it can be observed that, while the scaled control $\Gamma_\alpha(t)$ is not able to asymptotically stabilize the origin, it nevertheless provides a reduction of the oscillation of the limit cycle, see Fig. 10. This agrees up to a certain extent with the experimental results, where a reduction of the amplitude of the Rossiter peak is observed, instead of asymptotic convergence. It must be pointed out, however, that the experimental results show a much richer behavior of the controlled cavity flow in terms of the pressure fluctuations spectrum measured at the cavity floor, as the energy appears to be redistributed over a larger frequency range. The nonlinear analysis on the model (5.7) suggests also that a nonlinear control design which takes into account the presence of the actuator saturation might be a better alternative to conventional linear control methodologies. This direction will be pursued in our future work.

Figure 8 also indicates that the current reduced-order model based LQ control suppresses the third Rossiter mode, but the flow meanders around the second mode (rather than latching onto it as observed for some other linear controls). We believe that if our model was sufficiently rich (meaning that it was based on more cases than just Mach 0.3 baseline), this meandering around the second Rossiter mode would not have happened or wouldn't have been as noticeable.

## VI. Conclusions

The paper presents significant progress made by the flow control group at the Collaborative Center of Control Science at The Ohio State University in the development of reduced-order model based feedback flow control. The development and experimental testing of a closed-loop controller of the resonance of subsonic flow over a shallow cavity based on reduced-order models from experimental measurements are presented and discussed. The reduced-order model was obtained through the use of snapshot based Proper Orthogonal Decomposition (POD) of PIV data in conjunction with Galerkin projection of the Navier-Stokes equations onto the POD eigenfunctions. The stochastic estimation method was used for real-time estimate of the time coefficients of the model from dynamic surface pressure measurements. Equilibrium analysis led to the linearization of the reduced-order model around the equilibrium point. A simpler model for controller design was obtained by shifting the origin of the coordinates to the equilibrium point. This corresponds to removing the effect of the mean flow from the low-order model, and considering the local behavior of the system around the mean flow. The availability of real-time estimates of the state of the model allowed the use of linear state feedback control. To this aim we designed and tested experimentally a linear-quadratic optimal state feedback controller. From the results obtained we can conclude that the controller significantly reduces the resonance peak of the Mach 0.3 single-mode, for which it was designed, by switching it to a multi-mode resonance. The controller seems to be quite robust, as it can control the flow with some variations in the flow Mach number. It should be emphasized that these results while quite exciting are preliminary. Further analysis, interpretation, and development are forthcoming.

## Acknowledgments

This work is supported in part by the AFRL/VA and AFOSR through the Collaborative Center of Control Science (Contract F33615-01-2-3154).

The authors would like to thank Drs. James DeBonis and R. C. Camphouse, and James Malone, John Casey, Cosku Kasnakoglu, and Ryan Schultz for help and fruitful discussions.

## References


1. Adrian, R. J., "On the Role of Conditional Averages in Turbulent Theory," Turbulence in Liquids, Science Press, Princeton, 1979.
2. Adrian, R. J., and Moin, P., "Stochastic estimation of organized turbulent structure: Homogeneous shear Flow," *Journal of Fluid Mechanics*, Vol. 190, 1988, pp. 531-559.
3. Berkooz, G., Holmes, P. and Lumley, J. L. "The Proper Orthogonal Decomposition in the Analysis of Turbulent Flows." *Annual Review of Fluid Mechanics*, Vol. 25. 1993. pp. 539-575.
4. Bertsekas , D. P. *Dynamic Programming and Optimal Control*, Athena Scientific, 1995.
5. Caraballo, E., Samimy, M., and DeBonis, J., "Low Dimensional Modeling of Flow for Closed-Loop Flow Control," AIAA Paper 2003-0059, January 2003.
6. Caraballo, E., Malone, J., Samimy, M., and DeBonis, J., "A Study of Subsonic Cavity Flows - Low Dimensional Modeling," AIAA Paper 2004-2124, June 2004.
7. Cattafesta III, L. N., Williams, D. R., Rowley, C. W., and Alvi, F. S., "Review of Active Control of Flow-Induced Cavity Resonance," AIAA Paper 2003-3567, June 2003.
8. Cole, D. R., Glauser, M. N., and Guezennec, Y. G., "An Application of the Stochastic Estimation to the Jet Mixing Layer," *Physics of Fluids*, Vol. 4, No. 1, 1991, pp. 192-194.
9. Cole, D. R., and Glauser, M. N, "Application of Stochastic Estimation in the axisymmetric Sudden Expansion," *Physics of Fluids*, Vol. 10, No. 11, 1998, pp. 2941-2949.
10. Debiasi, M. and Samimy, M., "Logic-Based Active Control of Subsonic Cavity Flow Resonance," *AIAA Journal*, Vol. 42, No. 9, pp. 1901-1909, September 2004.
11. Debiasi, M., Little, J., Malone, J., Samimy, M., Yan, P., and Özbay, H., "An Experimental Study of Subsonic Cavity Flow – Physical Understanding and Control," AIAA Paper 2004-2123, June 2004.
12. Delville, J., Cordier, L. and Bonnet, J.P., "Large-Scale-Structure Identification and Control in Turbulent Shear Flows," In Flow Control: Fundamentals and Practice, edited by Gad-el-Hak, M., Pollard A. and Bonnet, J., Springer-Verlag, 1998, pp. 199-273.
13. Efe, M.Ö. and Özbay, H., "Proper Orthogonal Decomposition for Reduced Order Modeling: 2D Heat Flow," to appear in the Proc. of IEEE Int. Conf. on Control Applications (CCA'2003), June 23-25, Istanbul, Turkey, 2003a.
14. Efe, M.Ö. and Özbay, H., "Integral Action Based Dirichlet Boundary Control of Burgers' Equation," to appear in the Proc. of IEEE Int. Conf. on Control Applications (CCA'2003), June 23-25, Istanbul, Turkey, 2003b.
15. Gad-el-Hak, M., Flow Control – Passive, Active, and Reactive Flow Management, Cambridge University Press, New York, NY, 2000.
16. Glauser, M. N., Higuchi, H., Ausseur, J., and Pinier, J., "Feedback Control of Separated Flows (Invited)," AIAA Paper 2004-2521, June 2004.
17. Holmes, P., Lumley, J.L., and Berkooz, G., "Turbulence, Coherent Structures, Dynamical System, and Symmetry," Cambridge University Press, Cambridge, 1996.
18. Lumley, J. "The Structure of Inhomogeneous Turbulent Flows", Atmospheric Turbulence and wave propagation. Nauca, Moscow. 1967 166-176.
19. Murray, N., and Ukeiley, L, "Estimation of the Flowfield from Surface Pressure Measurements in an Open Cavity," *AIAA Journal*, Vol. 41, No. 5: technical notes, May 2003, pp. 969-972.
20. Picard, C., and Delville, J., "Pressure Velocity Coupling in a Subsonic Round Jet;" *International Journal of Heat and Fluid Flow*, Vol. 21, pp. 359-364, 2000.
21. Rowley, C. W., "Modeling, Simulation and Control of Cavity flow Oscillations", Ph.D. thesis, California Institute of Technology. 2002.
22. Samimy, M., Debiasi, M., Caraballo, E., Malone, J., Little, J., Özbay, H., Efe, M. Ö., Yan, P., Yuan, X., DeBonis, J., Myatt, J. H., and Camphouse, R. C., "Exploring Strategies for Closed-Loop Cavity Flow Control," AIAA Paper 2004-0576, January 2004.
23. Sirovich, L. "Turbulence and the Dynamics of Coherent Structures", *Quarterly of Applied Math*. Vol. XLV, N. 3, 1987, pp. 561-590.
24. Yuan, X. , Caraballo, E., Yan, P., Özbay, H., Serrani, A., DeBonis, J., Myatt, J. H. and Samimy, M., "Reduced-Order Model-Based Feedback Controller Design for Subsonic Cavity Flows", AIAA Paper 2005-0293, January 2005.

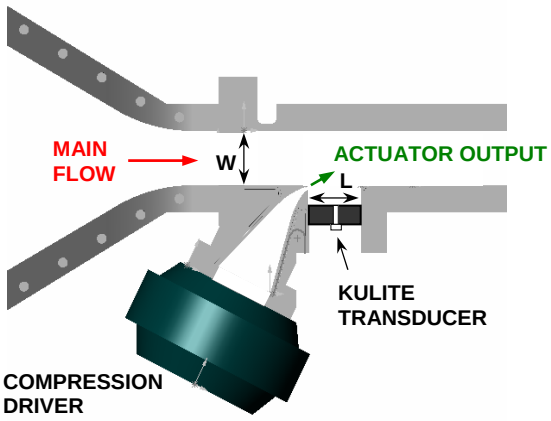


**Fig. 1: Scaled drawing of the experimental set up showing the incoming flow, the actuation location (at the receptivity location of the free shear layer formed over the cavity), and other geometrical details.**

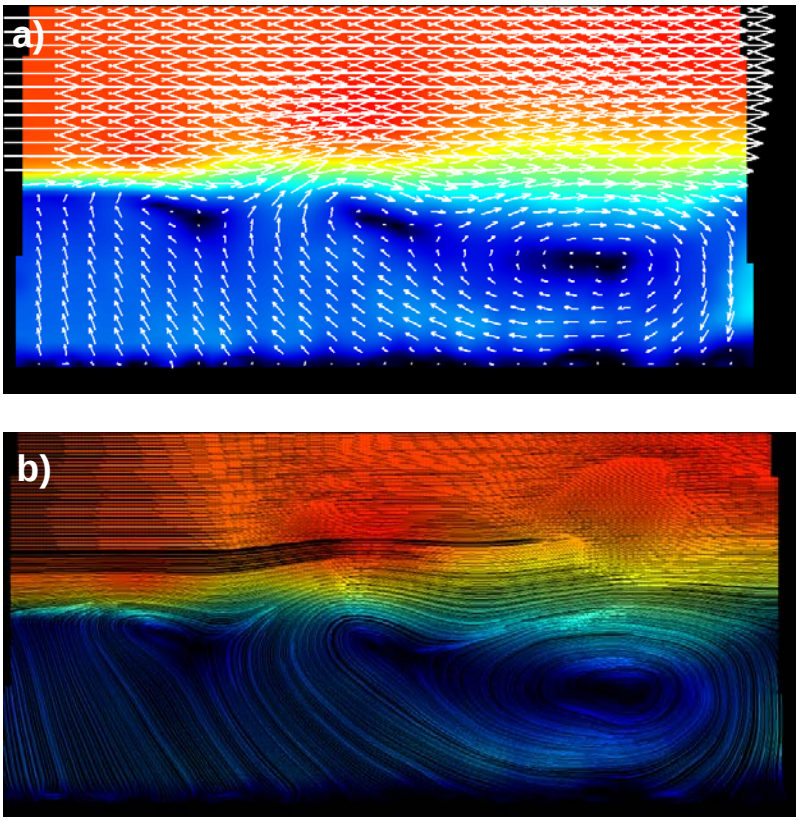


**Fig. 2: Phase-averaged PIV images of the Mach 0.30 flow over the cavity: a) vector field superimposed on an absolute velocity contour; b) streamlines.**


**Fig. 3: Location of Kulite pressure transducers in the cavity flow.**

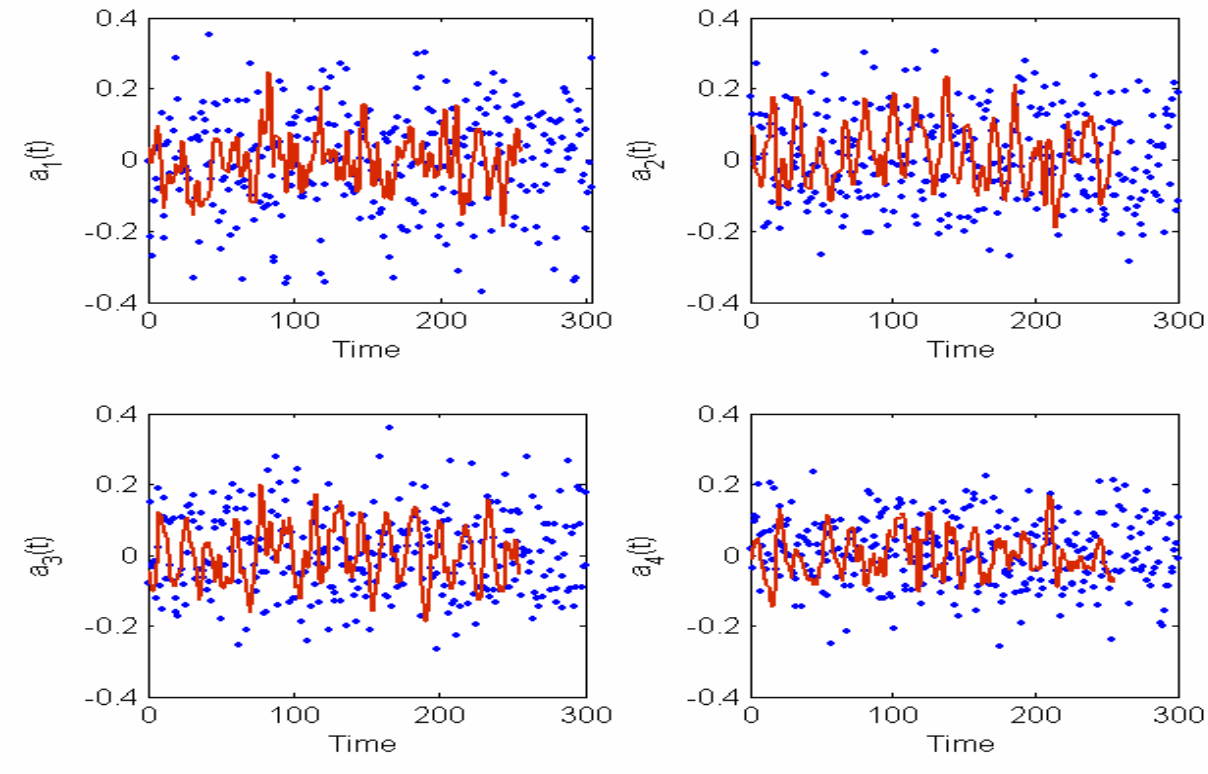


**Fig. 4: Estimated time coefficients from the surface pressure measurements. Red lines estimated, blue lines from PIV images.**

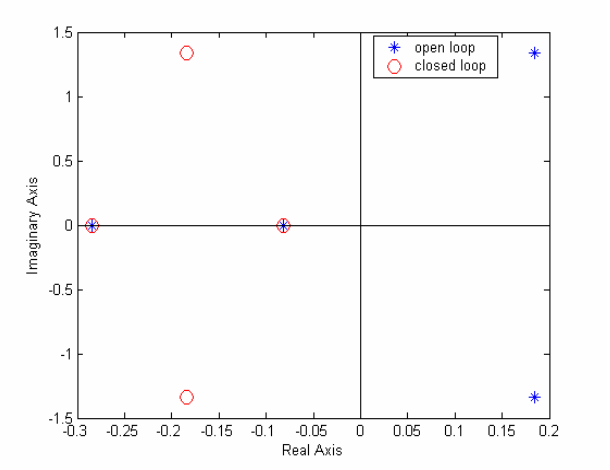


**Fig. 5: Eigenvalues of the open loop system and closed loop system.**

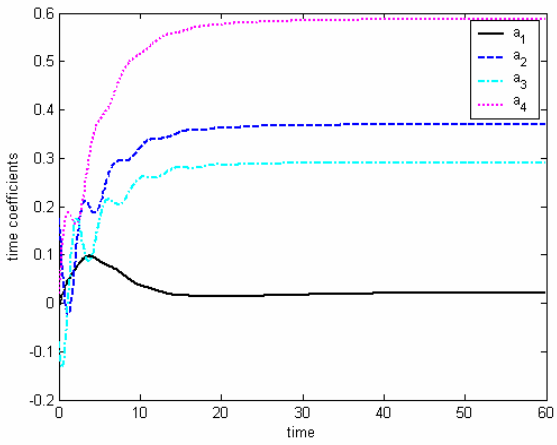


**Fig. 6: Time coefficient solutions of the closed loop simulation results.**

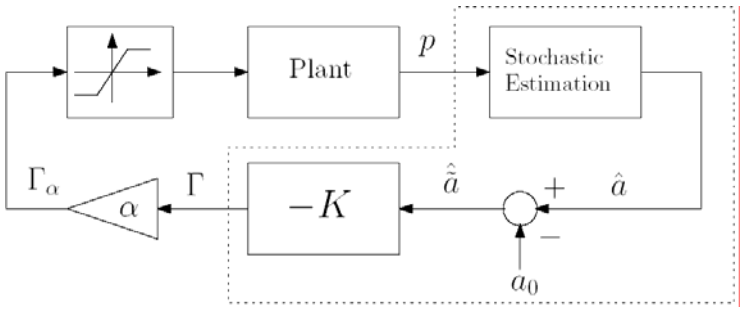


**Fig. 7: Diagram of the closed loop system with LQ state feedback control.**

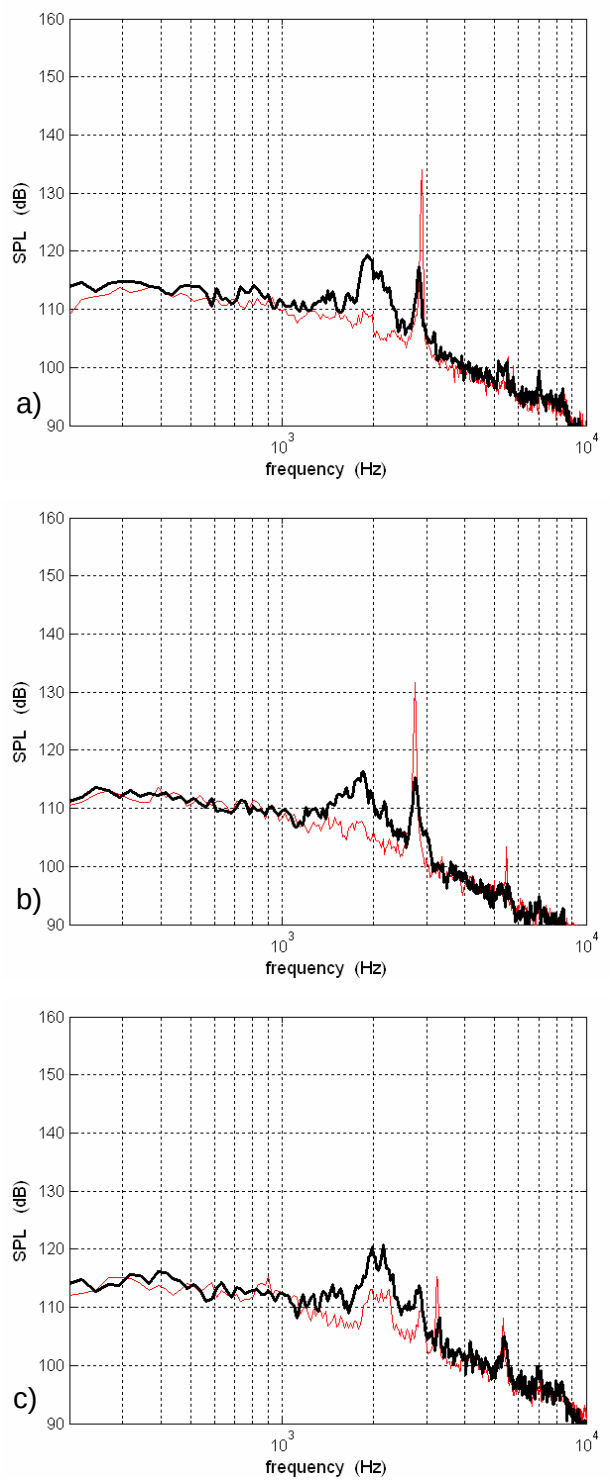


**Figure 8: Effect of LQ control with 4 modes on cavity flow with different Mach number; thin (red) line is the unforced flow SPL spectrum and thick (black) line is the spectrum with control at: a) Mach 0.30 (design condition); b) Mach 0.27; c) Mach 0.32.**

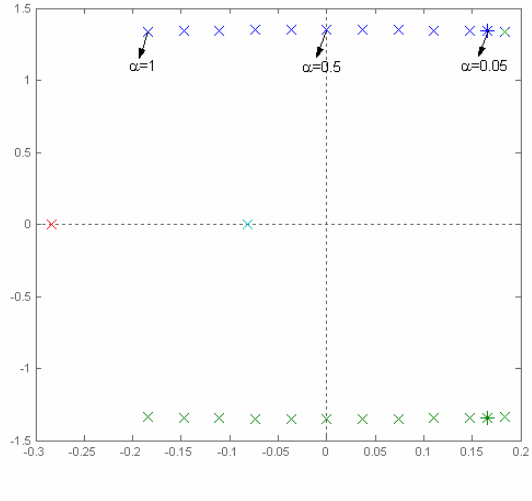


**Fig. 9. Eigenvalues of the closed loop systems with different scaling factor $\alpha$ .**

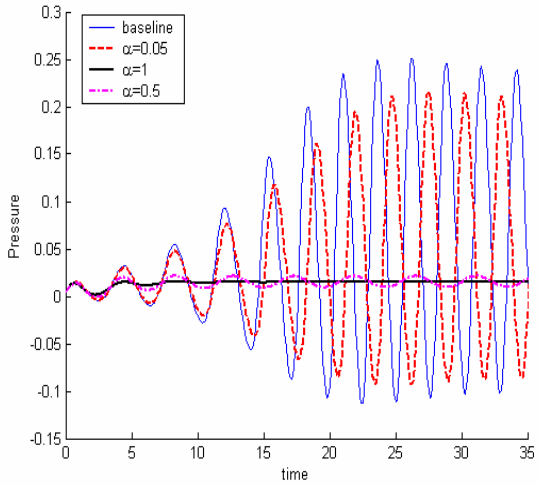


**Fig. 10: Closed loop responses at $P_3$ with different scaling factor $\alpha$ .**